A comparison of physics-based model computed and GNSS observed vertical land displacement of Greenland

Name	*Student number*
Mark Bemelmans	4365097

June 11, 2019

Abstract

By combining the RACMO2.3 RCM output with GRACE non-tidal ocean and atmospheric pressure anomaly as well as geo-center motion corrections from 2003 to 2017, a physics-based model to estimate the vertical displacement of the Greenland surface bedrock is created. This model is able to convert the mass and pressure anomalies into vertical displacement in the spherical harmonic domain with the use of load deformation coefficients based on the PREM earth model. The computed vertical displacement has a weak correlation with the observed displacement as measured by the GNET GNSS station network. Both the computed and observed vertical movement show seasonal signals, however the computed signal has both a lower amplitude and different phase to the observed displacement. This could possibly be explained by the selection of the GNET stations used in the analysis or possibly the implementation of the non-tidal ocean and atmospheric pressure anomaly. Questions regarding the optimization of the processing within the model are discussed but remain open. Recommendations for further research into the complexity of the system and shortcomings of the model are discussed in detail.

Name supervisor	*Research department*
Dr. P.G. Ditmar	Physical Space Geodesy
Dr. Ir. A.A. Verhagen	Mathematical Geodesy and Positioning

1 Preface

This research is part of my master education track Geoscience and Remote Sensing where it forms an Additional thesis. This research should be completed in roughly 280 hours of work. The project has been supervised by Dr. P.G. Ditmar and Dr. Ir. A.A. Verhagen to whom I am grateful for their guidance and support. I am also grateful for the use of code for part of the analysis provided by Pavel Ditmar, Yu Sun, Olga Didova, and Jainjun Ran.

Contents

2 Introduction

The paper goes into the interaction between the Greenland ice sheet and the solid earth. This topic is not often discussed because of the limited knowledge on the Greenland bedrock [Srokosz and Bryden, 2015]. The Greenland ice sheet does receive significantly more attention with several models dedicated to the evolution of the ice sheet, from thousands of years in the past like the ICE5G model [Peltier, 2004] to the daily 1x1 km regional climate model RACMO2.3 that focuses on the last 40 years since atmospheric observations are taken over the region [Noël et al., 2015], [internal communication with B. Noël]. This latter model will be used in this research because I focus on the contemporary changes to the ice sheet and the response from the solid earth.

Much is still unknown on the specific structure of the crust below the ice sheet, but the knowledge of the physical processes can still be applied. The main physical processes at play are the isostacy of Greenland and the ice sheet on the mantle below and elastic deformation of the crust. Variations of the surface loading causes lateral changes in overburden pressure at the lithosphere-asthenosphere boundary and causes flow of mantle material to form a new equilibrium to this new pressure distribution. This mantle flow causes deformation of the surface on the long timescale of thousands of years [Peltier, 2004]. Vertical deformation on timescales shorter than a year are not generally caused by the process of isostacy but rather the elastic deformation of the crust [Bevis et al., 2012].

The changes in the mass distribution of the Greenland ice sheet cause lateral pressure differences at the ice-crust interface. This leads to elastic deformation of the crust, especially in the vertical component. This vertical strain is observed in the movement of Global Navigation Satellite System (GNSS) stations located on the perimeter of the Greenland ice sheet and the coastal regions of Greenland [Bevis et al., 2012]. Elastic vertical crustal deformation due to ice mass change and the response to glacial isostatic adjustment has also been investigated by Zhang et al. [2017]; Groh et al. [2012] which are focussed on the antarctic ice sheets. The link between vertical deformation and surface load variation has also been researched by Chanard et al. [2014] who looked into the response of the crust in the Himalaya region to changes in seasonal continental water storage.

The mass of the Greenland ice sheet changes seasonally due to melting, refreezing, sublimation, and precipitation. This paper aims to provide additional information regarding the link between variations in surface loading and vertical displacement of the Greenland surface bedrock.

3 Problem statement

The total mass balance of the Greenland ice sheet (GrIS), displayed in figure 1, shows the superposition of two signals. First the approximately linear mass-loss rate of $286 \cdot 10^9$ tonnes per year and second a seasonal oscillating signal which has a yearly maximum in the late winter or early spring and a yearly minimum in late summer or early autumn.

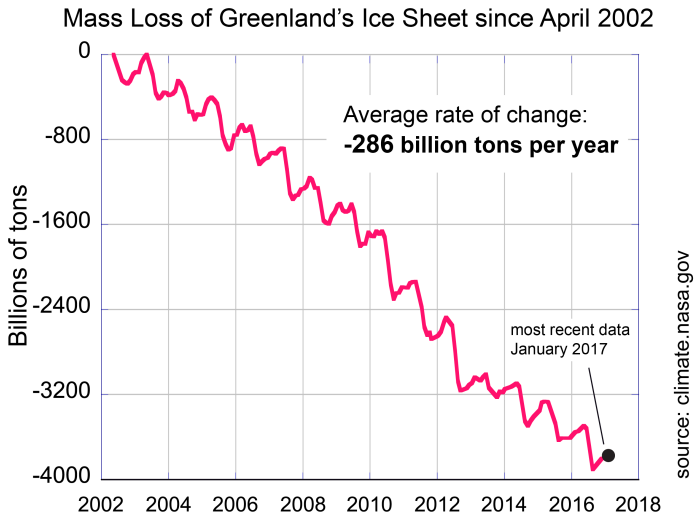

Figure 1: The NASA Gravity Recovery and Climate Experiment (GRACE) satellites detect changes in Earth's gravity, gravitational-change-based monthly estimate of the net mass change of Greenland's ice sheet since 2000. Sourced from: [climate.nasa.gov].

This research focuses on that seasonal signal as this is related to the short term changes of the ice sheet. These changes are caused by several processes of which the three most important for this research are: the accumulation of snow, the melting of ice/fern/snow, and the refreezing of the melted ice/fern/snow. The accumulation of snow in the winter adds mass to the ice sheet, the melting of material removes mass from the ice sheet and the refreezing of this melted material to ice compensates part of this mass loss.

A number of other processes cause pressure variations on the surface which can lead to vertical displacement of the land surface. These include the non-tidal ocean and atmospheric pressure variations and possibly the movement of the center of mass of the earth referred to as geo-center motion. The continent of Greenland responds to these seasonal mass and pressure variations by moving in the vertical. A positive displacement corresponds to a mass or pressure reduction at the bedrock surface as the overburden pressure is reduced, the reverse is also true where an increase in overburden pressure at the bedrock surface causes a negative displacement.

The main goal of this research is to accurately model the seasonal variations in the vertical displacement of the Greenland bedrock surface caused by physical processes and to evaluate this with the observed vertical displacement of the bedrock surface as measured by GNSS stations located at the perimeter of the Greenland ice sheet. The main research question is formulated as:

- Is it possible to combine the surface mass balance output of the RACMO2.3 regional climate model, non-tidal atmospheric and ocean pressure variation, and geo-center motion to create a model that can effectively estimate the vertical displacement measured at the GNET GNSS stations?

Dependent on the performance of the model, the possible missalignment and shortcomings of the model will be investigated to give recommendations for further research.

4 Data description

Four major data sets are used in this analysis. Firstly the available daily GNSS measurements from the network called GNET. Secondly, the Surface Mass Balance (SMB) model output from the RACMO2.3 regional climate model. Thirdly, the monthly atmospheric and ocean pressure anomaly field provided by the GFZ solutions to the GRACE mission. Finally, the monthly geo-center motion described by degree 1 spherical harmonic coefficients provided by [Sun et al., 2016]. In this chapter the four data sets are discussed in detail.

Additionally, the selection of the load love numbers, an important set of emperically derived values needed for the analysis, is discussed.

4.1 GNET: Greenland GNSS Network

GNET is a network of GNSS stations located along the coast of Greenland and all stations are attached to the bedrock of Greenland and are placed in order to study the displacement and deformation of the Greenland crust.

There are a total of 54 available GNSS stations all with a four letter/number identification code. A visual overview of the distribution of the stations can be found in figure 2.

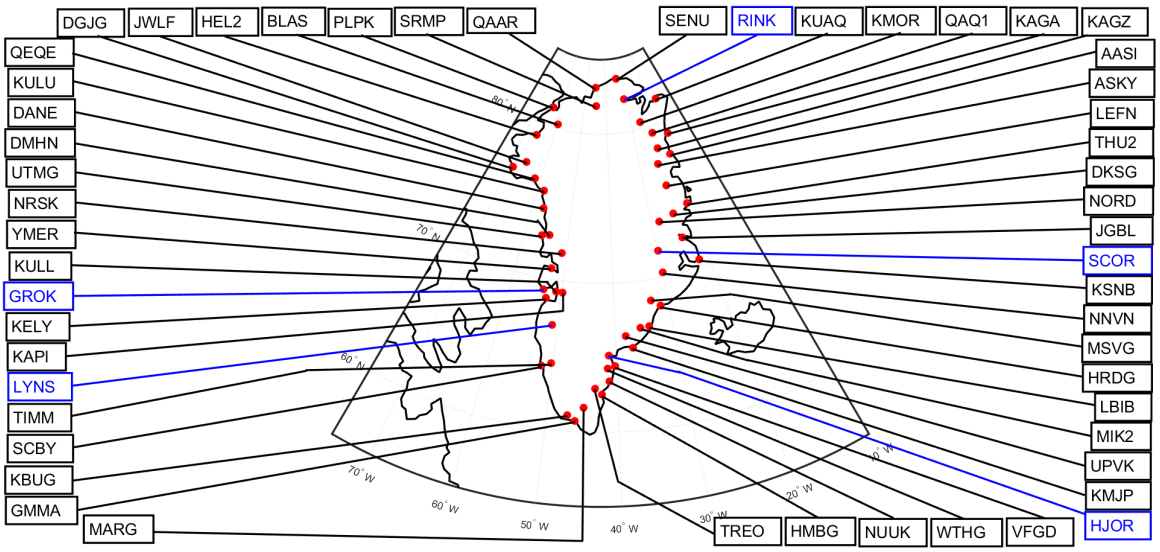

Figure 2: Spatial distribution of the GNET GNSS station for which data is available. The stations highlighted in blue are used as a subset for visual analysis.

The GNET network was formed by the installation of a significant number of stations in 2007, 2008, and 2009. Before that, only a handful of stations have data available. The stations measure their daily averaged position and record this. However, at times each station has a gap in the recordings which can complicate the analysis. Figure 3 shows the data availability for each of the stations.

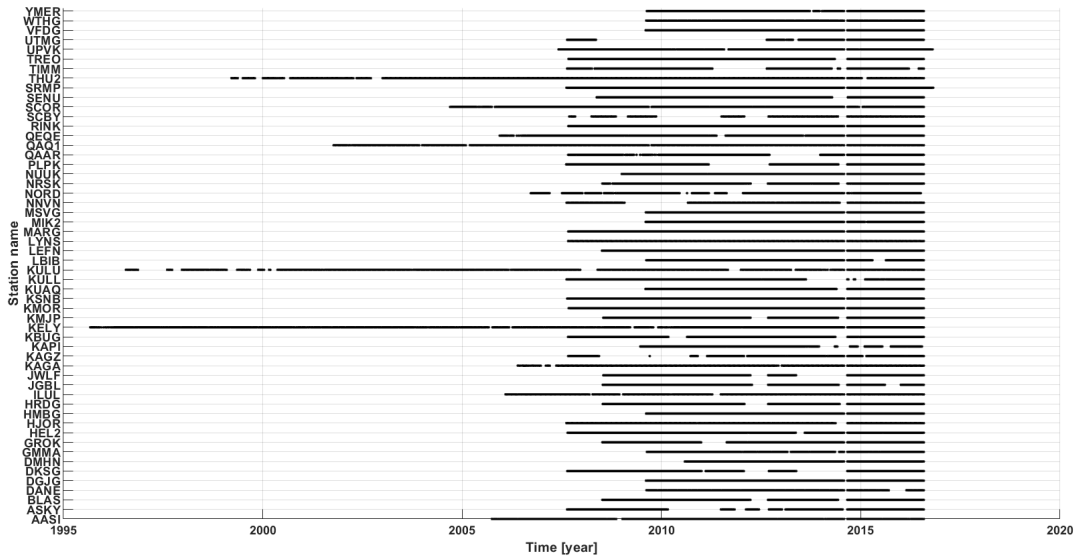

Figure 3: Temporal data availability per GNSS station. The presence of a black line indicates that data is available at that station.

Note the major increase in the number of available stations from 2007 onward. Also note that in 2014 there is a gap in the recording of every single station for approximately 3 weeks.

The data available at each station is comprised of the Eastward, Northward, and Upward displacement along with the 1σ uncertainty of that measurement given in mm [Khan et al., 2016; Bevis et al., 2009]. The scope of this research is limited to only the upward motion (and its uncertainty) of the GNSS stations. An example of this movement is presented in figure 4.

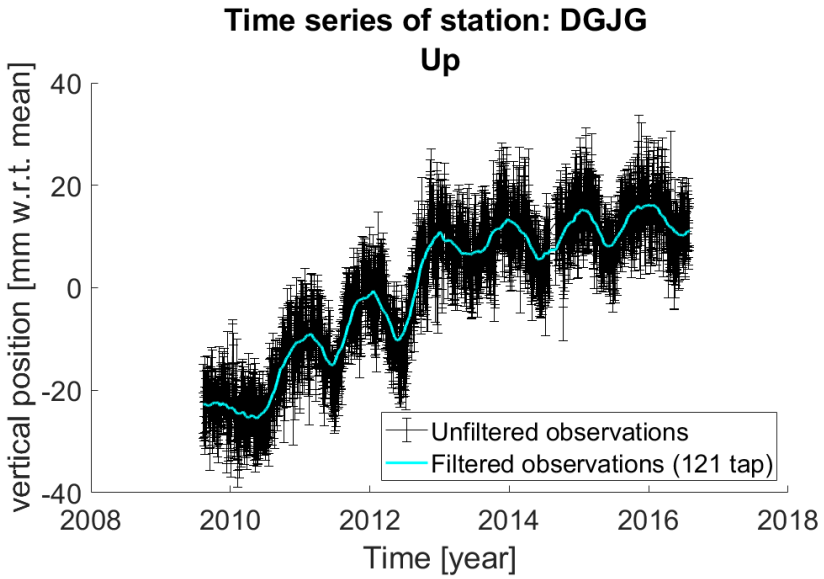

Figure 4: Example of GNSS time series showing the unfiltered signal with 1σ uncertainty (black) and the filtered signal (cyan).

This figure shows both the unfiltered measurements and the error-bars associated with each observation as well as the 121-tap moving average filtered measurements.

4.2 RACMO2.3 SMB output

RACMO2.3 is the latest version of a regional climate model (RCM) that focuses on the Greenland ice sheet. There is also a model for the southern hemisphere ice sheets, but this is outside the scope of this research. The model is able to provide output of the Surface Mass Balance, runoff, total melt [ice + snow], refreezing, total precipitation [rain + snow], snow drift erosion, sublimation and temperature 2 meters above the surface. The Surface Mass Balance or SMB is a generated variable and is given by equation (4.2.1).

$$SMB = Precipitation - (Melting - Refreezing) \tag{4.2.1}$$

This output is presented with a spatial resolution of 1x1 km and a daily temporal resolution. It should be noted that the spatial resolution has been increased from an 5.5x5.5 km resolution through statistical down-scaling. This allows the gradient in SMB to be resolved better, while not changing the underlying physics of the model [internal communication with Noël Bryce]. In this research the daily time interval, 1x1 km SMB output from the 1st of January 2003 to the 31st of December 2017 is used.

The Surface Mass Balance is only part of the mass balance of the Greenland ice sheet. The other major component in the mass balance is ice discharge to the ocean. This happens in the form of caving at the glacier fronts and direct melting at the ice-water interface. Another component in the overall mass balance of the ice sheet that is not taken into account by the SMB or by ice discharge, is the seasonal storage of meltwater. The current system for determining the mass of the ice sheet and therefore the load on the crust of Greenland does not include this storage of meltwater due to the limited understanding and complexity of this component. This has been extensively researched by Ran et al. [2018] which concluded that the signal is present in the mass balance of the ice sheet.

The coordinate system in which this gridded output is presented is WGS84 latitude and longitude values as well as NSIDC Sea Ice Polar Stereographic North or equivalently EPSG:3413. This is a convenient choice because the distortion caused by the projection is limited over Greenland. The latitude reference selected to have 1 m distance between every 1 unit value in the x direction is set to 70° which is roughly the mean latitude of Greenland.

4.3 Oceanic and atmospheric pressure anomaly

The Greenland ice sheet is not the only contributor to pressure variations at the surface of the bedrock. The ocean and the atmosphere also have seasonal pressure variations. The atmospheric pressure variations are discussed in [Bevis et al., 2012]. The data on the atmosphere and ocean pressure variations is obtained from models used by the Gravity Recovery and Climate Experiment (GRACE) which was in operation from March 2002 until October 2017. This satellite mission was used to produce detailed spatial and temporal observations to the Earth's gravitational field. A model is used to correct these oobservations for seasonal effects caused by pressure variation of the ocean and atmosphere. This research uses the AOD1B model described by Dobslaw et al. [2017b] to include the effects of ocean and atmospheric pressure variations on the vertical displacement of the Greenland bedrock. Over land this only concerns the surface pressure variations of the atmosphere and over the oceans this is the combined effects of the atmospheric and ocean pressures which result in ocean bottom pressure variations.

This product is supplied in the form of geo-potential spherical harmonic coefficients up to degree and order 180. The coefficients are provided for every month for which there is a GRACE solution available. The zeroth and first degree coefficients are ignored as these refer to the geo-center movement which are added separately. The coefficients describe the geo-potential anomaly with respect to the mean field from 2013-2014 which has been empirically calculated [Dobslaw et al., 2017a].

4.4 Geo-center motion time series

The GNSS stations get their reference from the positioning satellites and determine their position relative to the center of figure of the Earth. This is not the same as the center of mass of the Earth system because of mass movement near or on the surface of the Earth. The movement is comparatively small, however still a signal present in the observations that can be corrected for. The Geo-center motion is described by monthly values of the C_{10}, C_{11} and S_{11} Stokes' coefficients. These can be converted into vertical displacement using the load deformation coefficients [Sun et al., 2016].

4.5 Load deformation love numbers

The load deformation coefficients (LDCs) first described by A. E. H. Love is a set of numbers which collectively describe the response of the Earth to loading at the surface. There are three types of LDCs each describing a different aspect of the response. Only two of these are of concern for this research. The first are the (first) load deformation coefficients denoted by h'_l where subscript n gives the degree to which this number refers. The first load deformation coefficients are used to calculate the vertical movement caused by changes in the load potential. The second deformation coefficients (k'_l) describe the change in the gravitational potential due to the elastic deformation of the Earth. The degree 1 LDCs are dependent on the selected frame of reference [Blewitt, 2003]. Given the use of GNSS stations, the center-of-figure frame of reference is used and a correction of the geo-center motion is required. The degree 1 LDCs have been changed from the set referring to the ref6371 LDCs set presented by Melini et al. [2015] to the values presented in [Blewitt, 2003]. Another LDCs set created by Farrell [1972] was also used. This set however performed very poorly and is excluded from the analysis.

5 Method

The model will encompass three main physical processes: (surface) mass balance of the Greenland ice sheet, non-tidal ocean and atmospheric pressure anomaly and the geo-center motion. Each of these components require specific (pre-) processing steps to be converted to vertical displacement which can be compared to the observed displacement from the GNSS stations.

This section will go over all the processing steps required for all the separate components of the model as well as the visualization of the model output and the observed displacement.

5.1 Pre-processing of RCM output

The first step in the pre-processing of the RCM output is the conversion from the mass anomaly rate (given in mm equivalent water height per day) to an mass anomaly since the first day of output. This is done by firstly converting the equivalent water height (EWH) to mass anomaly per square meter. Here 1 mm EWH is equal to 1 $^{kg}/_{m^2}$. After this conversion the output is integrated through time setting the day before the first measurement as the zero mass anomaly epoch. Because the model output is given at daily intervals and the mass anomaly rate is given as mass anomaly per day, the integration simplifies to a cumulative summation through time.

The main processing part of the model output takes place in the spherical harmonic domain. This conversion requires data on a grid of dimensions (N+1)x2N spanning the entire globe where N+1 is the number of points in the latitudinal direction and 2N is the number of points in the longitudinal direction. The grid is taken such that the spatial distance between two points in the latitudinal direction is either 50 or 100 km. For this, the model output needs to be interpolated to the grid points. This is done using inverse distance weighting interpolation, where only the grid points that fall inside the region where model data is available are taken into account and only the model output within 100 km of the grid point are used for the interpolation. The interpolation powers used in the analysis are 2 and 3. This has the effect that the weight or importance of the data is related to the inverse of the squared (or cubed) distance of that data point to the interpolation grid point.

5.2 Processing of RCM output

The first step of the processing is the conversion of the RMC output from the spatial domain into the spherical harmonic domain. This is done using MATLAB functions provided by Olga Didova. The main component in this conversion is the Exact Neumann method for global spherical harmonic analysis which is described in detail in by [Sneeuw, 1994]. The global grid discussed earlier is needed to increase the precision of the global spherical harmonic analysis as described by the second Neumann method in [Sneeuw, 1994].

This conversion is a linear process and should therefore be easily reversed. There is however one issue in that the global spherical harmonic synthesis is only able to go up to a maximum degree which is obtained from the spatial resolution of the global Gaussian grid. This maximum degree is obtained using equation (5.2.1).

$$l_{max} = \frac{2\pi R_{Earth}}{\lambda} \tag{5.2.1}$$

In this equation l_{max} is the spherical harmonic degree needed to resolve features with a wavelength of λ. R_{Earth} is the mean radius of the Earth. In order to resolve features of wavelength λ, the sampling interval is required to be at least $\lambda/2$. The sampling intervals of 50 and 100 km resulting in maximum spherical harmonic degree values of 399 and 199 respectively are compared. It means that signals with wavelengths shorter than 100 km for the 50 km sampling and 200 km for the 100 km sampling are not resolvable and are therefore not taken into account when converting the data from the spatial to the spherical harmonic domain.

The model output is now in the spherical harmonic domain and can be converted from mass anomaly to vertical displacement. The first step in this conversion is to get the values from mass anomaly per square meter also called surface density anomaly to an anomaly in gravitational potential. This can be done by using equation (5.2.2).

$$\partial \bar{C}_{lm} = \frac{3(1+k_l')}{(2l+1)\tilde{R}\rho_{av}} \left(\frac{\tilde{R}}{R}\right)^l \bar{C}_{lm}^{(\partial s)} \tag{5.2.2}$$

Where $\partial\bar{C}_{lm}$ are the fully normalized spherical harmonic coefficients relating to the gravitational potential. $k_l^{'}$ are the second deformation load love numbers of degree l. l is the spherical harmonic degree. $\tilde{R}$ is the mean radius of the Earth while R is the radial distance from the center of the Earth to the observer. ρ_{av} is the average density of the Earth and finally, $\bar{C}_{lm}^{(\partial s)}$ are the fully normalized spherical harmonic coefficients related to the surface density.

For this application the radial distance to the observer is taken to be equal to the mean radius of the Earth which means that the conversion factor between the two sets of spherical harmonic coefficients is given in equation (5.2.3).

$$\frac{3(1+k_l^{'})}{(2l+1)\tilde{R}\rho_{av}} \tag{5.2.3}$$

The second step is to convert the spherical harmonic coefficients for the gravitational potential into spherical harmonic coefficients for vertical displacement. This is described in Groh et al. [2012] after the work of [Wahr et al., 1998]. Which describes a similar conversion factor to that of equation (5.2.3). This conversion is given in equation (5.2.4).

$$\bar{H}_{lm}^{ela} = \frac{h_l^{'}}{1+k_l^{'}}\tilde{R}\partial\bar{C}_{lm} \tag{5.2.4}$$

Here $h_l^{'}$ are the first deformation load love numbers of degree l and H_{lm}^{ela} is the set of fully normalized spherical harmonic coefficients relating to the vertical displacement. This creates the conversion factor:

$$\frac{h_l^{'}}{1+k_l^{'}}\tilde{R} \tag{5.2.5}$$

The direct conversion from mass anomaly to gravitational potential and then to vertical displacement is the same as the direct conversion from mass anomaly to vertical displacement. This can be done by using the product of the conversion factors. The problem thus reduces to equation (5.2.6). Additionally, positive mass anomaly values get converted to negative vertical deformation values. the GNSS stations take the 'UP' axis to be pointed perpendicular to the surface facing upward away from the surface. The LDCs are chosen positive/negative to let a positive mass anomaly result in a negative vertical displacement.

$$\bar{H}_{lm}^{ela} = \frac{3h_l^{'}}{(2l+1)\rho_{av}}\bar{C}_{lm}^{\partial s} \tag{5.2.6}$$

Note that the term $1+k_l^{'}$ is completely removed from this equation so the second deformation load love numbers are not required for this conversion. This equation is also present in Groh et al. [2012] where it is presented with the spherical harmonic coefficients of the rate of change in the surface density anomaly and the vertical displacement. By keeping the mass of the earth constant, the total mean gravitational potential at the surface will remain the same which means that $1+k_l^{'}$ does not need to be used in the calculation for vertical displacement.

The model output now describes the vertical displacement due to the mass change of the Greenland ice sheet, however it is in the spherical harmonic domain. In order to convert it back to the spatial domain, global spherical harmonic synthesis is applied. The MATLAB script for this was again provided by Olga Didova. To summarize, this script performs spherical harmonic expansion with the coefficients calculated above and evaluates them on the same (N+1)x2N global grid used before the transformation into the spherical harmonic domain. This final step results in a global map of vertical displacement since the first day of output with a daily time interval.

Lastly the resulting global grid of vertical displacement is interpolated to the locations of the GNSS stations by inverse distance weighing spatial interpolation using power values of 2 and 3 in the analysis.

There are two steps in the processing of the RACMO2.3 model data that include inverse distance weighting interpolation. There are two parameters in this interpolation that could significantly influence the outcome. Firstly the maximum distance from the interpolation point that the data should be used for the interpolation to that point. Secondly the power used in the interpolation. It was decided to compare two powers (2 and 3) for both interpolation steps as the power should have a significantly larger influence on the outcome than the maximum distance.

5.3 Processing of GNSS data

The GNSS data requires significantly less processing than the RACMO model output. The only problem with the GNSS data is that it is quite noisy which can make quantification of the seasonal signal difficult. In order to get some initial results, the vertical displacement data from every station is put through a moving average filter to reduce the noise. The moving average filter selected takes 31 adjacent observations, roughly equivalent to one month, averages these results and pins the averaged value to the central observation.

5.4 Optimization of interpolation methods and selection of maximum spherical harmonic degree

The inverse distance weighting spatial interpolation requires one interpolation parameter. The power which refers to the inverse relation between weight of the data point and the distance to that data point. When this power becomes larger, more of the weight is shifted to the closer data points. A smaller power distributes the weight more evenly over all data points. A standard value for the power is 2. However, since there is significant variability in the surface density anomalies near the coast (where the GNSS stations are located), It is assessed if a power value of 3 would be more applicable.

To this end, the analysis has been performed once for each option of the power value in the last interpolation step from the global grid to the GNSS locations. The first interpolation from the dense 1km x 1km grid of the Greenland ice sheet to the global grid has been kept at power 2 since the global grid should have an even balance between the contribution of large scale and small scale features.

There is a decision to be made in selecting the maximum spherical harmonic degree required in the analysis. Any signal with a wavelength shorter than the one described by equation (5.2.1) will not be taken into account in the analysis and the energy contained within these wavelengths is not properly taken into account. A comparison between a maximum spherical harmonic degree of 399 (50 km resolution) and 199 (100 km resolution) is made in order to assess if the spatial resolution is sufficient enough to capture the surface density anomaly signal properly.

5.5 Non-tidal atmosphere and ocean pressure anomaly

The AOD1B product obtained from GFZ is given for every month where a solution is present. In order to add this to the RACMO2.3 results, the AOD1B product needs to be interpolated to the same time epochs as the RACMO2.3 results. This is done by computing the mean day of the interval of the AOD1B solution and linearly interpolating each individual spherical harmonic coefficient between each solution. From there conversion factor (5.2.4) is used to convert the provided Stokes' coefficients to spherical harmonic coefficients for the vertical displacement. These are added to the same SH coefficients from the SMB data before the conversion to the spatial domain.

5.6 Correction for Geo-center motion

Geo center motion is the movement of the center of mass of the earth with respect to a predefined reference frame. In the case of GNSS stations this reference frame uses the center of figure (and not the center of mass) of the earth system as the origin. The movement of the center of mass result in changes to the geo-potential field of the Earth and can be expressed in terms of Stokes' coefficients [Sun et al., 2016]. Only the degree 1 Stokes' coefficients are needed to describe the geo-center motion. These coefficients presented by Sun et al. [2016] are converted to spherical harmonic coefficients for the vertical displacement and added to the spherical harmonic coefficients obtained after the non-tidal ocean and atmospheric pressure variation anomaly addition.

5.7 Comparison of model and data

For every station location there is now a set of time series of vertical displacement derived from the regional climate model, non-tidal oceanic and atmospheric pressure anomaly, and geo-center motion and a second set of time series that was measured by the GNSS stations. In order to compare the data, the model output is interpolated to the GNSS data disregarding any GNSS measurements before 2003. Next the linear trend from both time series are removed as this is assumed to be the result of glacial isostatic adjustment from the last glacial maximum (LGM) as well as contemporary ice discharge which also causes mass loss to the ice sheet which would both result in an upward vertical displacement rate. What remains are two signals which should be similar.

5.8 Comparison of model output

Up to now there are three models used. Firstly the model which only takes the time integrated surface mass balance and converts this to vertical displacement. Secondly, the model that adds the signal for the non-tidal ocean and atmospheric pressure anomaly. Finally, the model that adds the signal for both the non-tidal ocean and atmospheric pressure anomaly and the geo-center motion. From the interpolation optimization the best result is taken and used for further analysis. This analysis takes the computed vertical displacement time series at the station location and linearly interpolates these results to the time epochs of the measured vertical displacement of that station. Additionally some stations appear to show a multi-year trend. In order to compare the level of fit on the seasonal signal, the multi-year trend is isolated by subtracting a moving mean over 731 (2 year) observations from the signal. This is done for both the observations as the time interpolated computed values to be able to equally compare them. From there, the multi-year average at the day of year is computed for all the time series and this result is averaged over all the stations to get one result for the entire island. This helps identify any general shortcomings of the model to describe the seasonal signal in vertical displacement of the Greenland bedrock surface. Additionally, A least square fit with an annual and semi-annual oscillation is taken of these results in order to identify the phase and amplitude of the (semi-) annual oscillation. The model is described by the matrix equation (5.8.1).

$$\begin{bmatrix} 1 & cos(2\pi t_1) & sin(2\pi t_1) & cos(4\pi t_1) & sin(4\pi t_1) \\ 1 & cos(2\pi t_2) & sin(2\pi t_2) & cos(4\pi t_2) & sin(4\pi t_2) \\ \vdots & \vdots & \vdots & \vdots & \vdots \\ 1 & cos(2\pi t_n) & sin(2\pi t_n) & cos(4\pi t_n) & sin(4\pi t_n) \end{bmatrix} * \begin{bmatrix} x_1 \\ x_2 \\ x_3 \\ x_4 \\ x_5 \end{bmatrix} = \vec{y} \tag{5.8.1}$$

Where t_i is the time given in decimal year, x_i are the model parameters and $\vec{y}$ are the various time series. The phase and amplitude of the signal can then be visualized in a phasor plot.

6 Description and interpretation of results

The analysis results in time series of the modelled vertical displacement and the filtered measured displacement at the location of the GNSS stations. These two signals should, in theory, be highly correlated. The initial assessment of the correlation between the modelled and measured vertical displacement is performed visually.

This section will go over the comparison and selection of the spatial resolution of the spherical harmonic analysis followed by the analysis of the optimal inverse distance weighting interpolation parameters. The comparison of the different models occurs thereafter and the chapter closes with generalized results for the entire island.

This step-by-step process is followed to show the process of decision making with regards to some of the model parameters. The additions to correct for other seasonal signals is done separately after the determination of the model parameters. Due to time constrains of this work, it was not possible to perform quantitative analysis on the level of fit for the selection of the model parameters.

6.1 Selection of maximum spherical harmonic degree

The maximum spherical harmonic degree determines to what detail the available data is resolved on a global scale. The more information is available, the more accurate the data processing is. The processing has been performed with a latitudinal resolution of 50 km and 100 km which refer to a maximum spherical harmonic degree to 399 and 199 respectively. The first thing that changes between the two situations is the density of the grid points at which the spherical harmonic expansion can be resolved. The grid of these two situations is provided in figure 5.

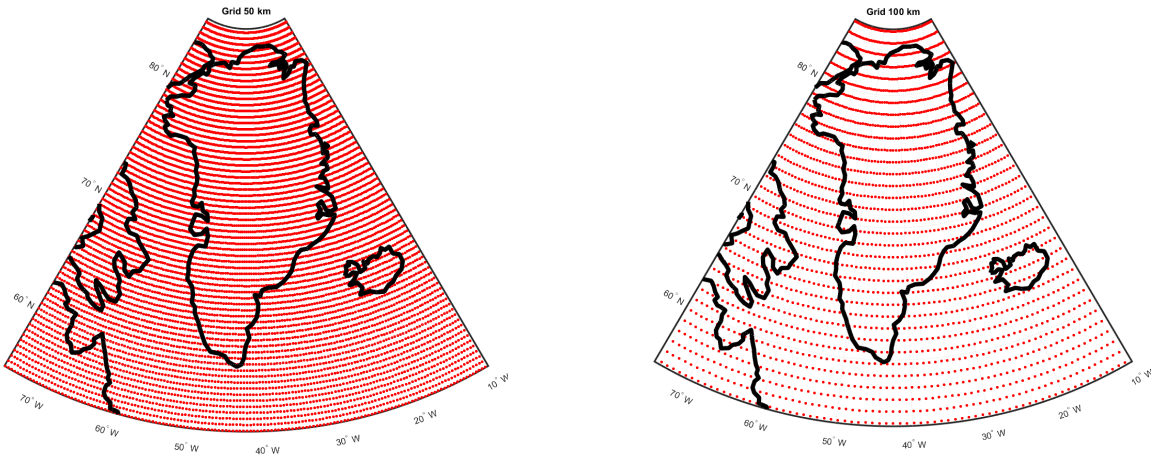

(a) grid 50 km resolution

(b) grid 100 km resolution

Figure 5: Grids associated with maximal spherical harmonic coefficient degree 399(a) and 199(b) respectively.

From the figure it is observed that the grid density is about four times as high with the 50 km resolution compared to the 100 km resolution. The availability of data can influence the results when interpolating especially when only data points within a certain distance to the interpolation point are considered.

This results in a time series at each of the 54 GNSS station locations. A few stations have been selected to provide an overview of the available results these stations are highlighted in figure 2.

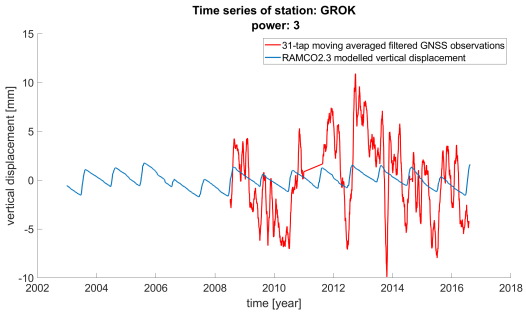

(a) GROK location resolution 50 km

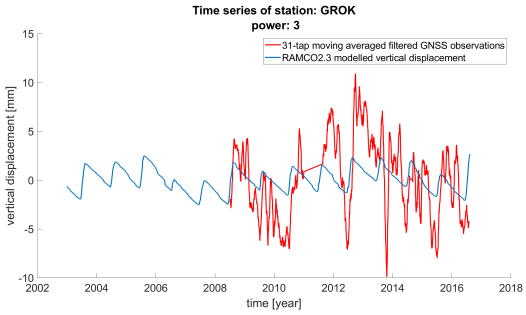

(b) GROK location resolution 100 km

Figure 6: Time series of GROK station associated with maximal spherical harmonic coefficient degree 399(a) and 199(b) respectively.

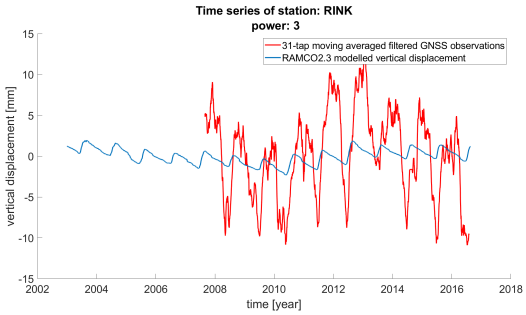

(a) RINK location resolution 50 km

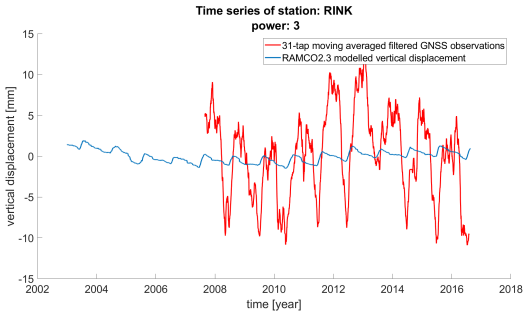

(b) RINK location resolution 100 km

Figure 7: Time series of RINK station associated with maximal spherical harmonic coefficient degree 399(a) and 199(b) respectively.

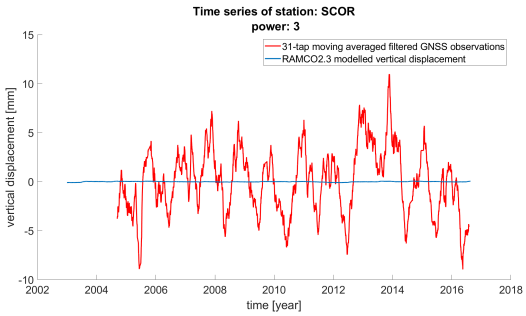

(a) SCOR location resolution 50 km

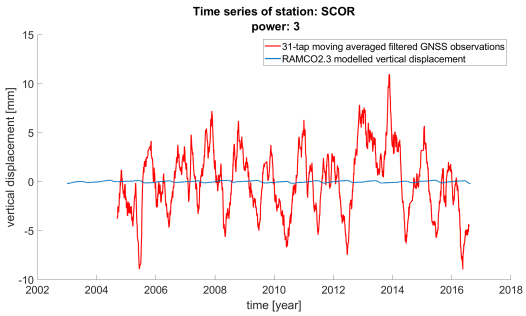

(b) SCOR location resolution 100 km

Figure 8: Time series of SCOR station associated with maximal spherical harmonic coefficient degree 399(a) and 199(b) respectively.

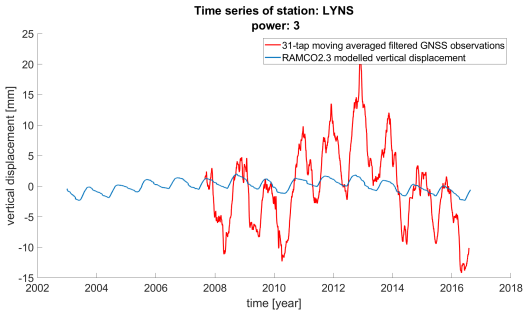

(a) LYNS location resolution 50 km

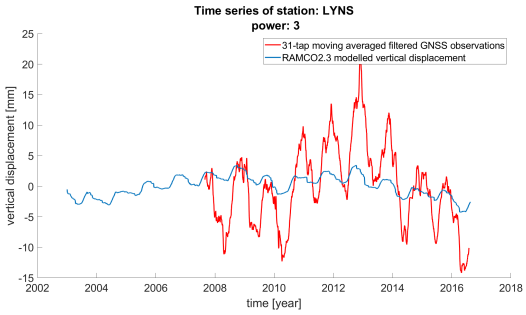

(b) LYNS location resolution 100 km

Figure 9: Time series of LYNS station associated with maximal spherical harmonic coefficient degree 399(a) and 199(b) respectively.

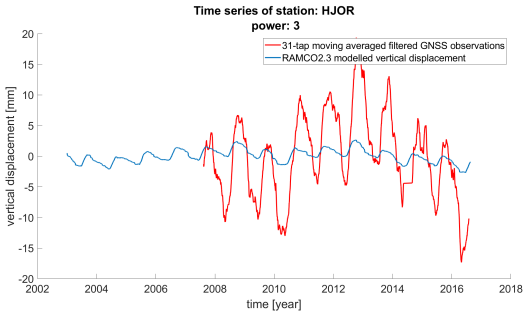

(a) HJOR location resolution 50 km

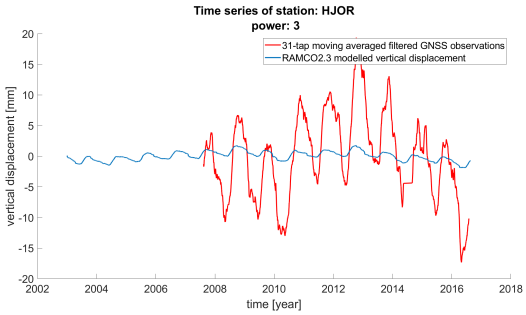

(b) HJOR location resolution 100 km

Figure 10: Time series of HJOR station associated with maximal spherical harmonic coefficient degree 399(a) and 199(b) respectively.

From this selection of stations, the following six points have been observed. Firstly, the GNSS signal has a significantly larger amplitude in the seasonal signal compared to the computed vertical displacement independent of resolution or location. Secondly, from station GROK it is observed that not every station has a clear seasonal signal in the GNSS observations. Thirdly, the calculated vertical displacement shows a seasonal signal in most stations, but as observed from station SCOR this is not the case everywhere. Fourth, a phase difference is observed between the observed vertical displacement and the calculated vertical displacement where the observed vertical displacement shows a lag of ¼ of a year. This results in the maximum value of the calculated vertical displacement corresponding with the maximum (positive) slope of the measured vertical displacement. The calculated displacement has a peak in the autumn and slowly transitions to a local minimum at the end of spring. This is followed by an often rapid change to positive displacement over the summer months, coinciding with the melting season of the Greenland ice sheet. Fifth, the linear detrending operation to remove the effect of GIA from the LGM and current ice discharge shows that the measured vertical displacement at some stations show second (and higher) order polynomial terms as evidenced by the crest-like shape in the observations of station LYNS and HJOR. Finally, it is of note that the stations GROK and LYNS are in somewhat close proximity to one another as seen in figure 2. There is little to no similarity in the measured displacement between the two stations. The signal of LYNS better resembles that of HJOR. This leads to think that there are other contributors to the vertical displacement which when combined result in a large multi-year signal that acts on a large spatial scale combined with a large seasonal signal that is spatially more variable.

Now for the difference between the two resolutions as a result of the selection of the maximum spherical harmonic degree. A general statement regarding the differences between the two resolutions cannot be made. At stations GROK and LYNS the 100 km resolution has a slightly stronger seasonal signal compared to the 50 km resolution results. At the stations RINK and HJOR the signal of the 50 km resolution is slightly stronger than the 100 km resolution. The station SCOR shows no significant signal in both the 50 and 100 km resolutions There is a very weak seasonal signal present in the 100 km resolution. Looking at all 54 stations the amplitude of the computed signal is slightly but noticeably higher, on average, with the 100 km resolution compared to the 50 km resolution. Because of this and the shorter computation time, further analysis is done with the 100 km resolution.

The reason for this might be that there is a significant amount of noise present in the SMB data on the wavelength scales

between 200 and 100 km. The computed displacement is also saw-tooth shaped for nearly all the locations which seems to be a result of the rapid melt in spring and summer and steady but slower accumulation during autumn and winter. This model output is not resembling the more sinusoidal seasonal trend observed in the measured displacement. The phase of the measured vertical displacement is different from the computed displacement for this SMB only model. One simple explanation is given by assuming that the observed displacement is the result of the superposition of several signals that are not completely in phase with each other. The 100 km resolution model provides the higher level of fit and will be used for further analysis. An analysis of the original data and the conversion to the spherical harmonic domain might provide additional information on the reason why the maximum spherical harmonic degree of 199 slightly outperforms the results obtained from the maximum degree 399 model.

6.2 Selection of interpolation parameters

Another aspect in the processing is the selection of the power value used for the inverse distance interpolation. The power value of 2 and 3 are compared with each other in the figures of the stations GROK, RINK, SCOR, LYNS, and HJOR in figures 11 - 15.

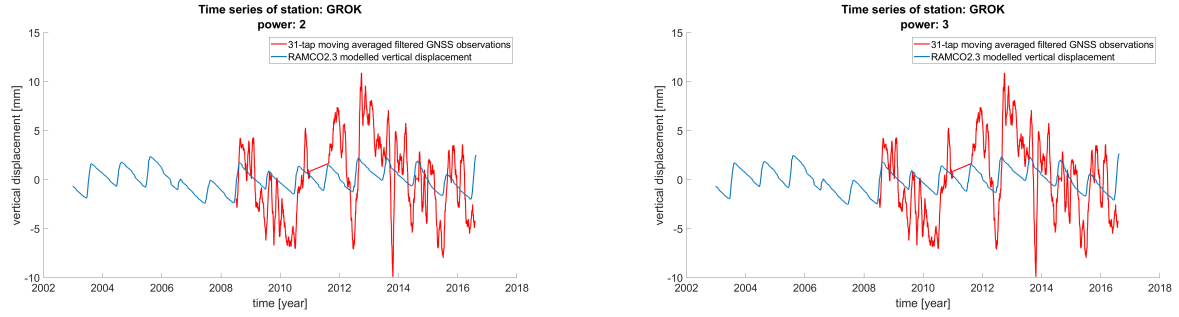

(a) GROK location (power 2)

(b) GROK location (power 3)

Figure 11: Time series of stations GROK associated with the interpolation power value 2(a) and 3(b).

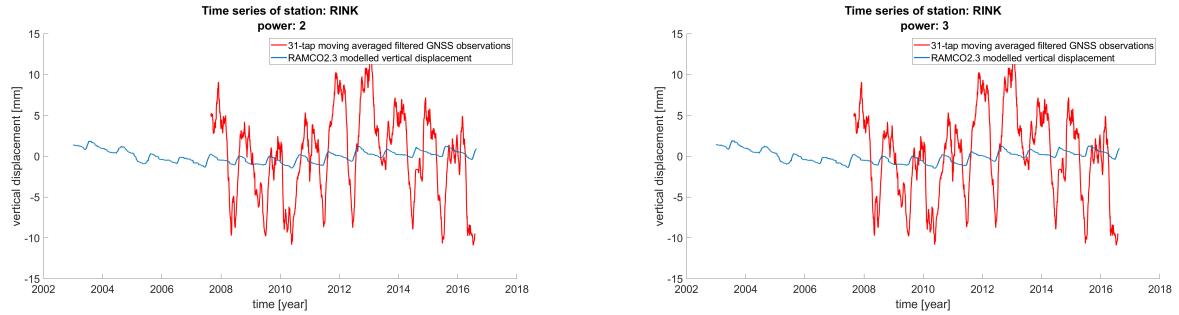

(a) RINK location (power 2)

(b) RINK location (power 3)

Figure 12: Time series of stations RINK associated with the interpolation power value 2(a) and 3(b).

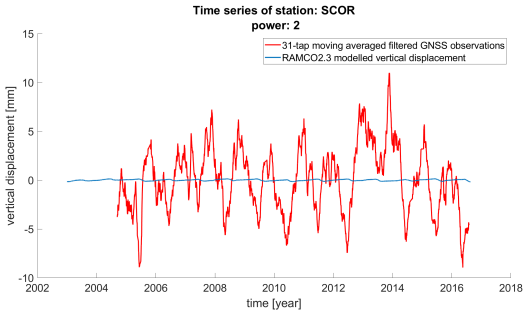

(a) SCOR location (power 2)

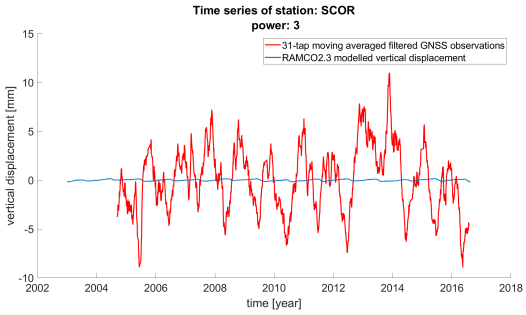

(b) SCOR location (power 3)

Figure 13: Time series of stations SCOR associated with the interpolation power value 2(a) and 3(b).

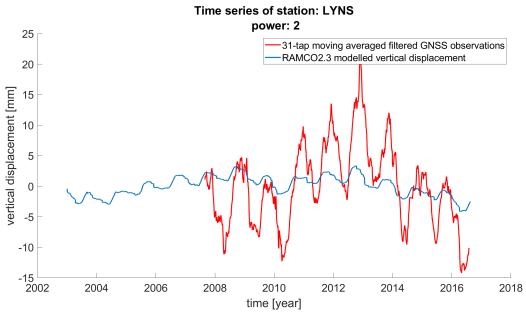

(a) LYNS location (power 2)

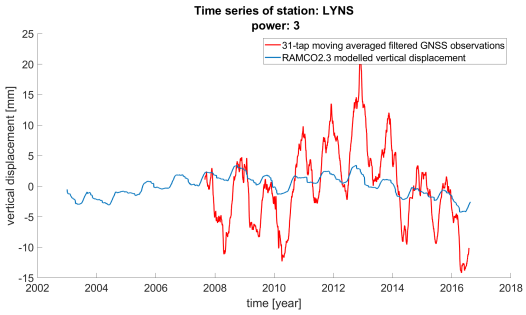

(b) LYNS location (power 3)

Figure 14: Time series of stations LYNS associated with the interpolation power value 2(a) and 3(b).

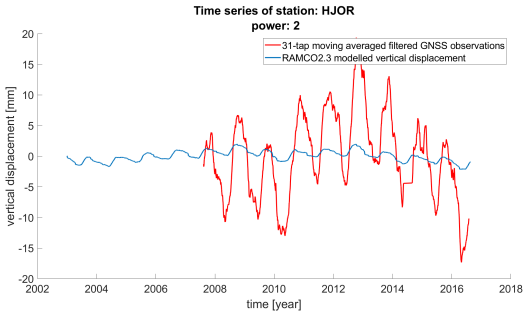

(a) HJOR location (power 2)

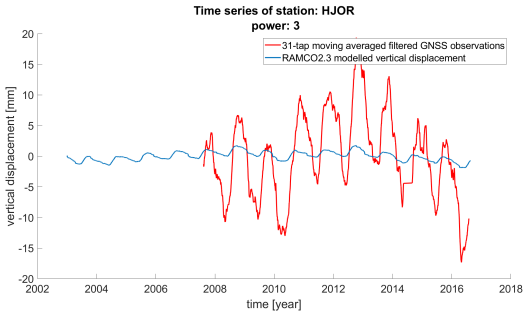

(b) HJOR (power 3)

Figure 15: Time series of stations HJOR associated with the interpolation power value 2(a) and 3(b).

No significant difference in the shape of the computed vertical displacement is observed between the power 2 and power 3 computed vertical displacement. The choice of the interpolation parameter does not affect the computed displacement. Further analysis is done with the inverse distance interpolation power 3. Like before with the resolution, there might be an optimal value to be used which could be found with further analysis on the spatial variability of the model output and the observed displacement.

Overall, the seasonal signal in the computed displacement has a significantly lower amplitude than the measured displacement. This result was not expected from Ran et al. [2018] where the seasonal signal from RACMO2.3 is comparable to that of the GRACE mass anomaly product. Now the GRACE mass anomaly product is not the same as the vertical displacement of the GNSS stations but the disparity in signal strength between the computed and measured displacement is an interesting topic for further research.

6.3 Addition of non-tidal atmospheric and oceanic pressure anomalies

The atmosphere and ocean surrounding Greenland exert pressure on the air-ice and air-land interface for the atmosphere and at the ocean bottom for the ocean and atmosphere combined. Seasonal changes in weather patterns, ocean circulation and (northern hemisphere) ocean volume result in seasonal pressure variations much like those caused by the ice sheet. These have been added to the model and are compared to the 100 km resolution, power 3 model without the addition in figures 16 - 20.

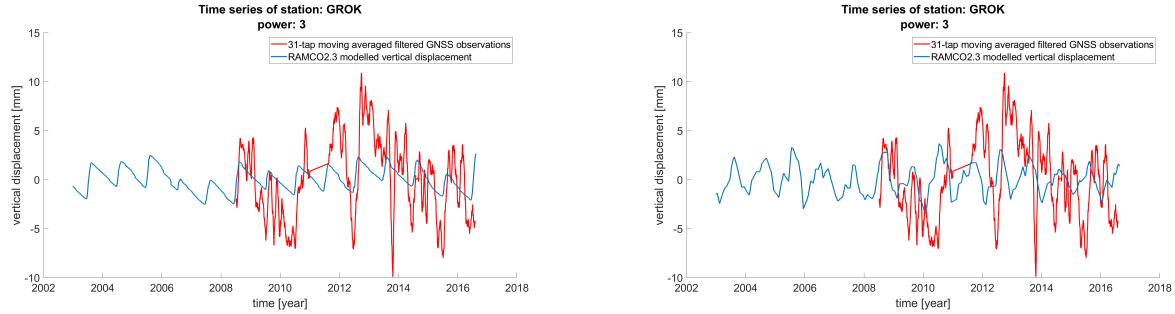

(a) GROK location (no addition)

(b) GROK location (ao addition)

Figure 16: Time series of stations GROK comparing the SMB only (a) and ocean + atmosphere added (b) models.

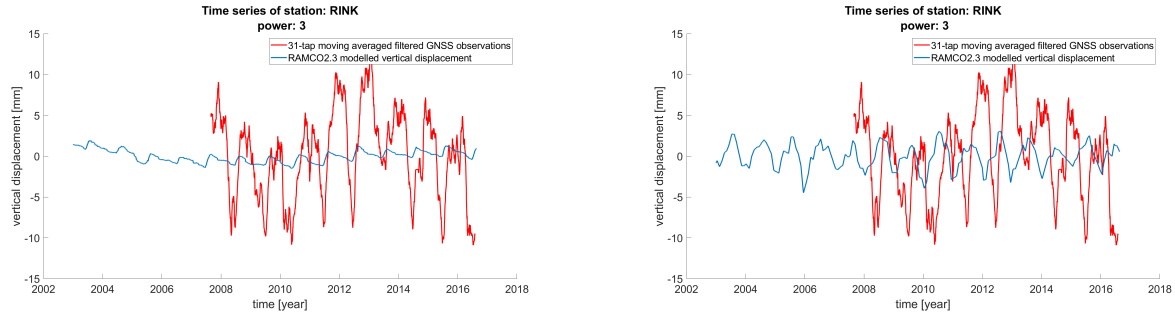

(a) RINK location (no addition)

(b) RINK location (ao addition)

Figure 17: Time series of stations RINK comparing theSMB only(a) and ocean + atmosphere added (b) models.

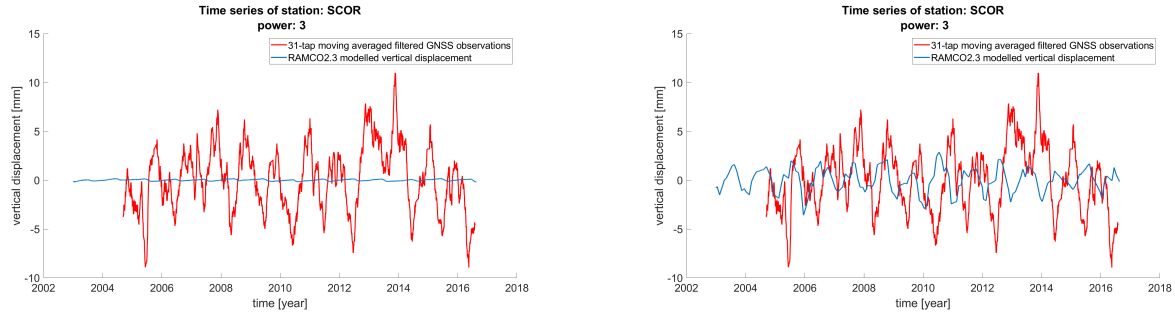

(a) SCOR location (no addition)

(b) SCOR location (ao addition)

Figure 18: Time series of stations SCOR comparing the SMB only (a) and ocean + atmosphere added (b) models.

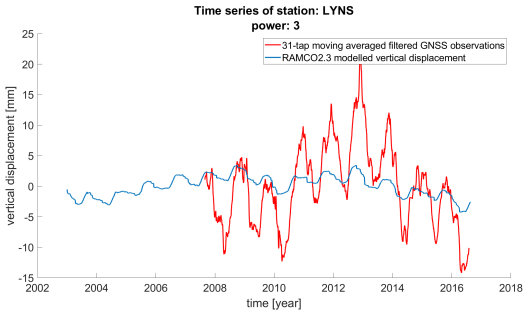

(a) LYNS location (no addition)

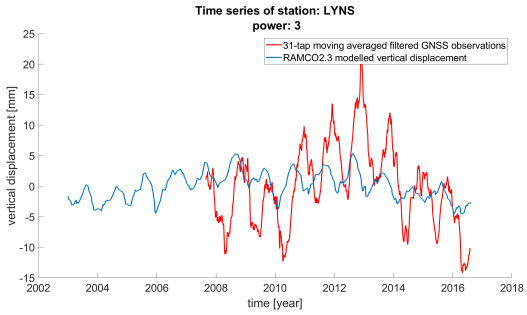

(b) LYNS location (ao addition)

Figure 19: Time series of stations LYNS comparing the SMB only (a) and ocean + atmosphere added (b) models.

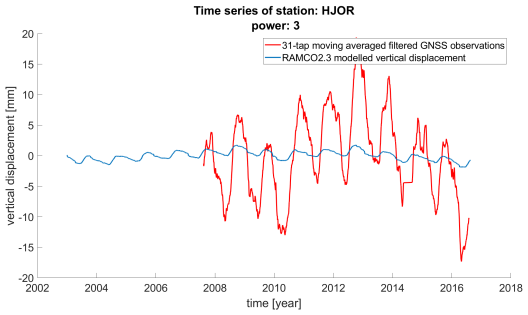

(a) HJOR location (no addition)

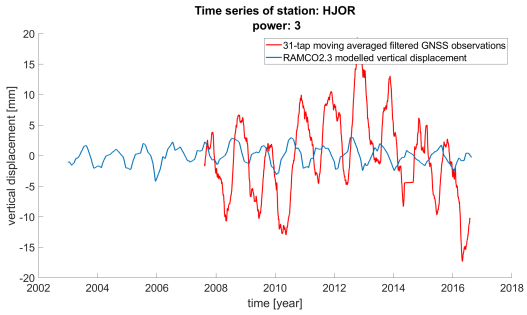

(b) HJOR location (ao addition)

Figure 20: Time series of stations HJOR comparing the SMB only (a) and ocean + atmosphere added (b) models.

The figures show a significant increase in the strength of the seasonal signal for the computed vertical displacement. A phase shift is observed in all the stations after applying the non-tidal ocean and atmospheric pressure anomaly addition. Furthermore, comparing the computed signals from the stations shows that the ocean and atmosphere pressure addition has largely reduced the spatial variability and the stations now have similar calculated displacement. The seasonal signal of the computed displacement at stations RINK, LYNS, and HJOR is of significantly lower strength than that of the observed signal. This is due to those stations having a larger amplitude seasonal signal in the measured displacement compared to stations GROK and SCOR.

The difference in phase of the annual signal between the computed and measured displacement seem to go against the findings of [Bevis et al., 2012]. That research added the signal from GRACE, which according to Ran et al. [2018] is comparable to the RACMO2.3 SMB output after correcting for ice discharge, and the air mass signal from the MM5 polar weather model to get a highly correlated combined mass signal to the GNET averaged displacement signal. [Bevis et al., 2012] did however not convert this mass signal to vertical deformation. Additionally, neither the MM5 weather model nor the GRACE mass anomaly product include seasonal changes in ocean bottom pressure which are included in the GRACE ocean and atmosphere correction used in this research. The connection between the separated ocean and air components to the movement of the GNSS stations is an interesting topic for further research.

6.4 Geo center motion correction

The motion of the center of mass of the Earth has an effect on the vertical displacement measured at the GNSS locations. To compare these results to those obtained earlier, the modelled displacement without additions; with only the non-tidal ocean and atmospheric pressure correction; and with both the non-tidal ocean and atmospheric pressure correction and the correction for geo-center motion are visualized together with the observed displacement at the previously selected stations. This is presented in figures 21 to 25. All results were obtained using a resolution of 100 km and an IDW power of 3.

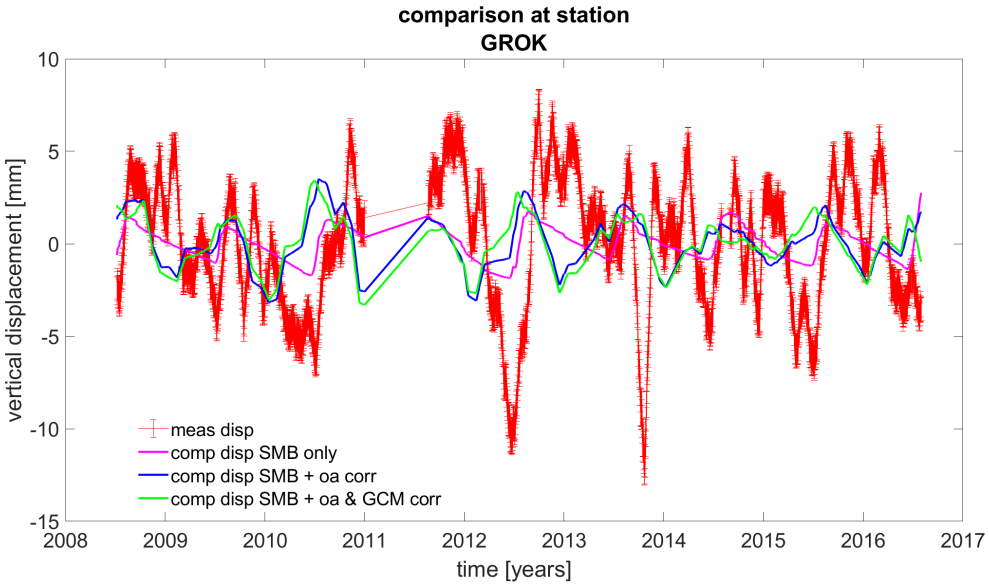

Figure 21: Comparison of model output and observations for the GROK station

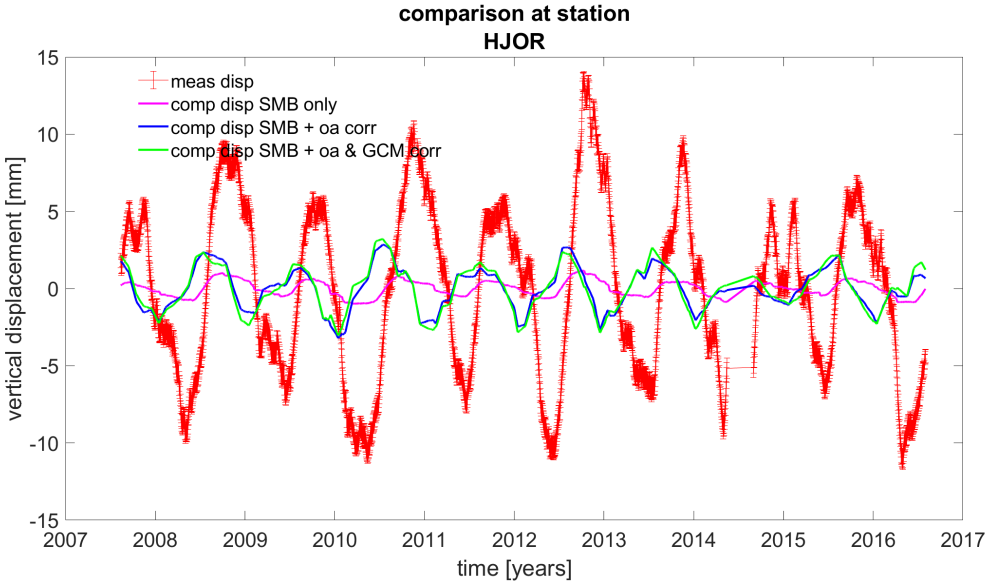

Figure 22: Comparison of model output and observations for the HJOR station.

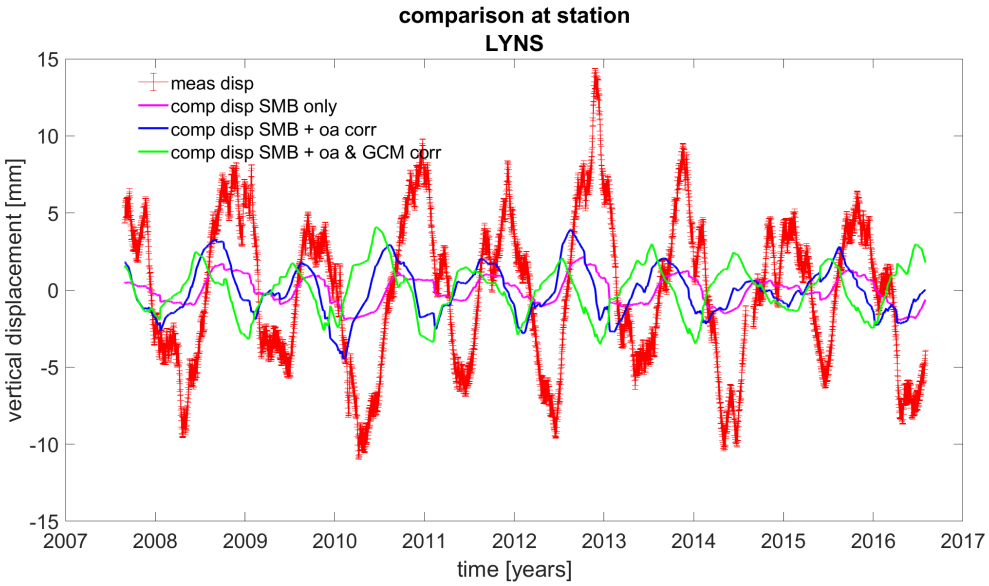

Figure 23: Comparison of model output and observations for the LYNS station.

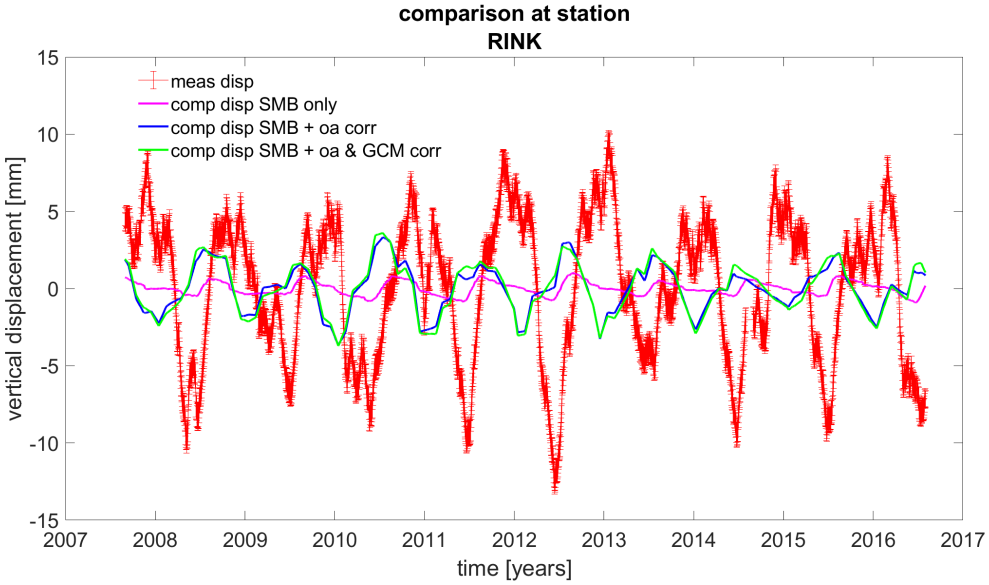

Figure 24: Comparison of model output and observations for the RINK station.

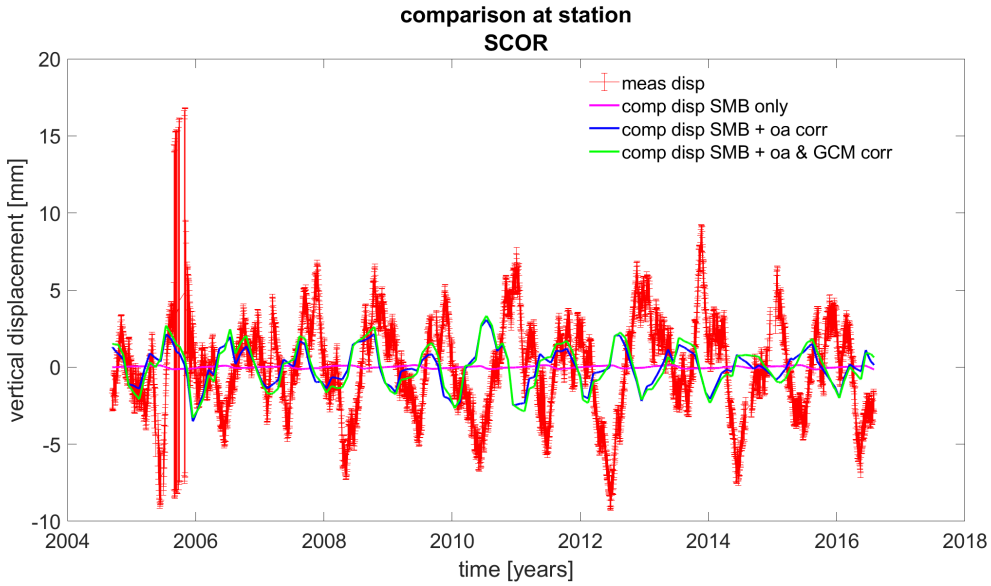

Figure 25: Comparison of model output and observations for the SCOR station.

The addition of the geo-center motion does not significantly change the shape to the computed displacement for most stations. For station LYNS the geo-center motion causes a phase shift in the computed signal towards the observed displacement.

6.5 Seasonal signal analysis

This research is mainly focused on the seasonal signal present in the vertical displacement. Each time series is averaged for it's day of the year value. Afterwards, this result is averaged over all the 54 locations to get one value for the entire island. This is presented in figure 26. The results are presented with downward (down) as the positive direction to be similar to the figure presented in [Bevis et al., 2012].

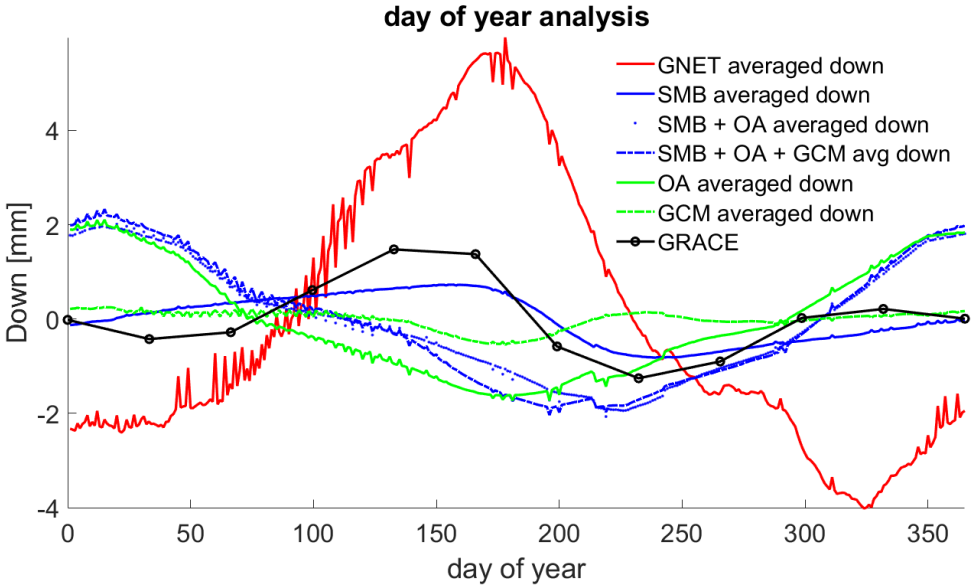

Figure 26: Greenland seasonal signal comparison.

This figure confirms that the seasonal signal of the measured displacement is significantly stronger than the computed displacement regardless of the model used. The maximum downward measured displacement takes place roughly 180

days into the year. The SMB only model shares this aspect with the observations. The GRACE data reaches a maximum about a month earlier at day 150. The SMB and ocean and atmosphere pressure anomaly model peaks in the beginning of the year at day 10. This is mostly due to the ocean and atmosphere pressure anomaly which peaks at the same time. The GRACE data and the RACMO SMB results are similar in shape, but the GRACE data shows a clear semi-annual cycle. The phase and amplitude are computed from the matrix equation (5.8.1). This is visualized in figure 27 and 28.

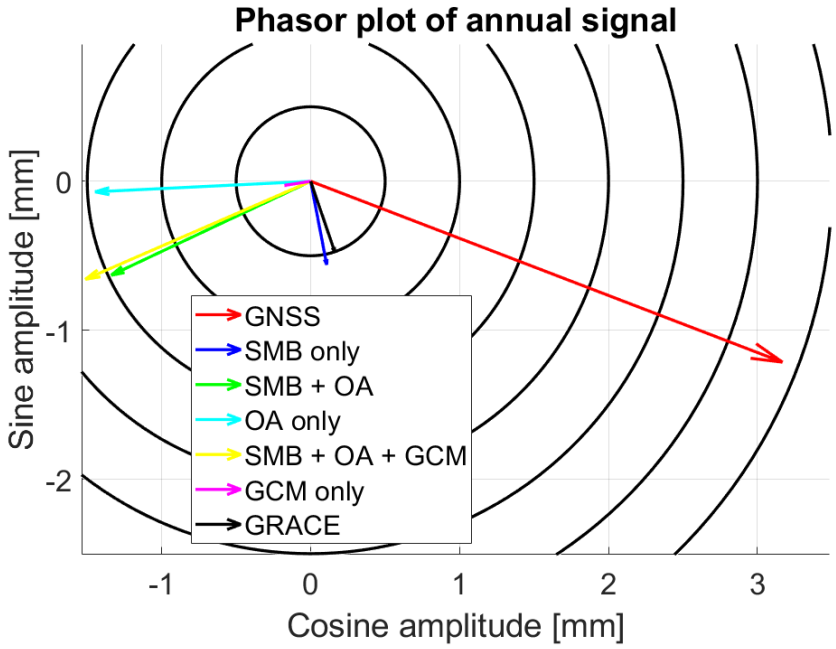

Figure 27: Phasor plot of the annual oscillation. The angle of the vector from directly right going counterclockwise, indicates the phase of the signal. The concentric rings indicate amplitude and are 0.5 mm apart.

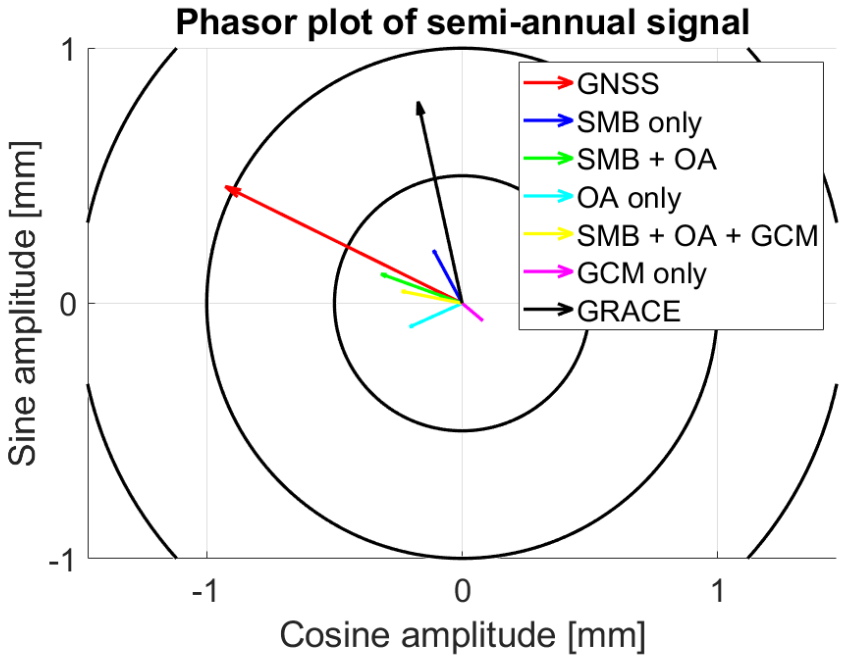

Figure 28: Phasor plot of the semi-annual oscillation. The angle of the vector from directly right going counterclockwise, indicates the phase of the signal. The concentric rings indicate amplitude and are 0.5 mm apart.

From figures 27 and 28 it can be observed that the phase of the annual oscillation from the various models are quite dissimilar. Especially when compared to the GNSS time series. The phase of the SMB only and GRACE annual oscillations are very similar and the amplitude is similar as well at about 7 times smaller than the GNSS time series. The ocean and atmosphere addition is significantly larger in amplitude but the phase of the annual signal is in nearly the opposite direction to the GNSS time series. The phase of the semi annual oscillation is roughly in the same direction for the models and the observations. However, apart from the GRACE data, all of the models show very small amplitudes for the semi-annual oscillation. This is not surprising as the semi-annual signal in the observations is 3 times weaker than the annual signal. From both figure 27 and 28 the geo-center motion is a very weak signal and has a near opposite phase to the GNSS measured displacement. No analysis is preformed on the residuals between the observed and computed displacement because of the phase difference.

7 Discussion

The difference in phase and amplitude makes analysis of the residuals unnecessary. In this chapter the status of the model is described in detail. The inconsistencies with the observed displacement are discussed as well as the inconsistencies with the literature on this topic. Possible explanations for the inconsistencies are given and expended on to provide an initial direction for further research.

7.1 Findings from the model

The model including the signal from the SMB of the Greenland ice sheet, non-tidal oceanic and atmospheric pressure anomalies and geo-center motion does not highly correlate with the observations. This is mainly due to differences in the phase and amplitude. The simplest explanation for the difference in amplitude is that there is another component missing in the model which has a great effect on the vertical displacement. This would have to be a signal at least as strong as the combined signal from the model components as it is now.

There is one clear candidate for a missing component that is responsible for a large part of the observed seasonal oscillation in vertical displacement. This is the movement of the bedrock due to water that gets into the cracks and fractures of the bedrock and expands when freezing. This expansion can cause significant movement of the bedrock surface. Murton et al. [2006] shows that freezing pore water can cause bedrock heave of up to 10 mm. This is dependent on the depth of the fractures and the temperature conditions at the bedrock. It is well within the realm of possibility for the bedrock of Greenland, especially the coastal regions where temperature variation is highest, to have fractured and filled with pore water which freezes each year and expands. This would cause uplift in the winter which is what is observed from the GNET GNSS stations.

In comparing the results of this work with those of Bevis et al. [2012], it is of note that they did not convert the ice and air mass signals to vertical displacement. This means that not much can be said on the amplitude of the combined signal. Additionally, the paper is from the year 2010 which only provided the authors with about 3 years of data from most of the GNET stations. The peak in my re-creation of the GNSS Down signal, using all available data up to 2018, is shifted significantly further to the summer.

7.2 Comparison of RACMO2.3 SMB output and GRACE ice mass signal

From figure 26 a relatively large difference between the vertical displacement of the RACMO2.3 SMB model and the GRACE mass anomaly product is observed. This is larger than is expected from Ran et al. [2018] where the SMB signal of the entire ice sheet and the GRACE mass anomaly product are mostly in line, but apart from the seasonal meltwater storage that was the main focus of that research. Since nearly the same data is used, the most likely reason is the relatively low number of spatial data points used in the analysis. The 54 distributed GNSS stations are only able to capture a small part of the processes of the ice sheet that are present in the original RACMO2.3 SMB output and the GRACE mass anomaly product. This shows that there are spatial differences between the GRACE mass anomalies and the RACMO2.3 SMB output interpolated to the GNSS station locations. It also suggests that the results interpolated to the station locations, which are later combined into one result, are not representative of the behaviour of the ice sheet or even that of the vertical movement of the bedrock surface. The selection of the GNSS stations might also significantly influence the results from this figure.

8 Conclusion

The results make clear that the physical implementation of the RACMO2.3 SMB, non-tidal oceanic and atmospheric pressure anomaly and geo-center motion does not result in vertical displacement at the locations of the GNET GNSS station that strongly correlates with the observed vertical displacement from the stations. Therefore it is concluded that a model purely based on RACMO2.3 SMB, non-tidal oceanic and atmospheric pressure anomaly and geo-center motion Is not able to effectively model the vertical deformation of the Greenland bedrock surface. The modelled displacement does show inconsistencies with the observations and other external data which show insight into the shortcomings of this model and leads to further research. The inconsistencies with respect to literature can be attributed to the selection of stations and the addition of data recorded after the publication of the literature in question. There are several actions which can be taken to investigate these inconsistencies which are described in the next chapter.

9 Recommendations for further research

9.1 Optimal maximum spherical harmonic degree

The SMB data obtained from the RACMO2.3 RCM is provided at a resolution of 1x1 km covering the ice sheet. In this research this is converted to a global grid with a latitudinal resolution of 100 km. A significant amount of the shorter wavelength structures in the SMB of the ice sheet is lost in this conversion. A resolution of 50 km was also tested which performed slightly less well than the 100 km resolution. The energy present at these shorter wavelengths that are not included might have some none-neglectable effect on the vertical displacement calculation. Therefore, both the variability of the spherical harmonic coefficients in time and from one degree/order to the next, might be able to provide insight into the optimal maximal spherical harmonic degree.

9.2 Optimal interpolation parameters

As concluded, there is no observable difference between the power 2 and power 3 interpolation parameter for the inverse distance weighting interpolation. This however, does not exclude that the selection of this parameter is trivial and has no impact on the output of the model. There might be an optimal value somewhere outside the 2-3 range. Additionally, there are better, but admittedly much slower, interpolation methods such as kriging that might improve the accuracy of the processing step. One could check the validity of the interpolation step by performing leave-one-out cross validation, where one point from the input is left out and is used as query point for the interpolation to later be checked against the original value.

9.3 Spatial variability of RACMO2.3 vs GRACE

The significant difference in the GNET averaged computed vertical displacement from the SMB model and GRACE mass anomaly data shows that there are some possible issues with the GNET averaging of the results. This can be investigated by taking a subsection of the GNSS stations for the analysis. Some of the stations are located at the edge of the ice sheet while others are located near the coast. This research might also be able to provide more information on the possible differences in the vertical displacement between the two types of stations or any other division of the stations (e.g. drainage regions, North vs South, East vs West). Alternatively, the difference could also lie in the original data itself. Since the GNET averaged values act as a value for the entire ice sheet, one could use the original RACMO2.3 SMB data and the GRACE data over the ice sheet to compute the ice sheet averaged mass anomalies. These should according to Ran et al. [2018] be nearly identical apart from the quite linear ice discharge not present in the SMB data and the relatively small seasonal melt water storage signal present in the GRACE data.

9.4 Bedrock uplift caused by freezing pore water

The difference between the computed and observed vertical displacement might be explained by the expansion of freezing water in the fractures and other pore-space present in the bedrock This freezing would cause an uplift in the order of 10 mm [Murton et al., 2006]. The Greenland bedrock is among the oldest on earth and have been extensively reworked [Andresen et al., 2007; Leslie et al., 2008; Patchett et al., 1978]. It is therefore completely possible that fractures in the

bedrock have been filled with water which and expands during winter when it freezes, causing uplift. To the knowledge of the author, modelling of the uplift has not been performed before for the Greenland bedrock. This needs to be done in order to effectively model the seasonal vertical displacement pattern shown in the observations by the GNET GNSS stations.

9.5 Radial structure of the Greenland mantle and crust

Every set of inputs into the model gets converted to spherical harmonics of the vertical displacement by use of the Load Deformation Coefficients (LDCs). These are constructed from our best understanding to the radial structure of the Earth. However, this radial structure beneath Greenland is not well known. Additionally, the Earth is not spherical nor perfectly radially symmetric. This can cause changes of the LDCs which will surely alter resulting in vertical displacement. The use of a LDCs set that is more representative of the conditions found beneath Greenland will surely improve the accuracy of the results.

References

Andresen, A., Rehnström, E., and Holte, M. (2007). Evidence for simultaneous contraction and extension at different crustal levels during the caledonian orogeny in ne greenland. *Journal of the Geological Society*, 164(4):869–880.

Bevis, M., Kendrick, E., Brown, A., Khan, S., Knudsen, P., Madsen, F., Wahr, J., and Willis, M. (2009). Greenland gps network: Crustal oscillations and seasonal ice mass fluctuations. In *AGU Fall Meeting Abstracts*.

Bevis, M., Wahr, J., Khan, S. A., Madsen, F. B., Brown, A., Willis, M., Kendrick, E., Knudsen, P., Box, J. E., van Dam, T., et al. (2012). Bedrock displacements in Greenland manifest ice mass variations, climate cycles and climate change. *Proceedings of the National Academy of Sciences*, 109(30):11944–11948.

Blewitt, G. (2003). Self-consistency in reference frames, geocenter definition, and surface loading of the solid Earth. *Journal of geophysical research: solid earth*, 108(B2).

Chanard, K., Avouac, J., Ramillien, G., and Genrich, J. (2014). Modeling deformation induced by seasonal variations of continental water in the Himalaya region: Sensitivity to Earth elastic structure. *Journal of Geophysical Research: Solid Earth*, 119(6):5097–5113.

Dobslaw, H., Bergmann-Wolf, I., Dill, R., Poropat, L., and Flechtner, F. (2017a). GRACE AOD1B Product Release 06: Long-Term Consistency and the Treatment of Atmospheric Tides. In *EGU General Assembly Conference Abstracts*, volume 19, page 10136.

Dobslaw, H., Bergmann-Wolf, I., Dill, R., Poropat, L., and Flechtner, F. (2017b). Product description document for AOD1B Release 06 (Rev. 6.1). Technical report, GRACE Document 327-750, Technical report. GeoForschungsZentrum Potsdam.

Farrell, W. (1972). Deformation of the Earth by surface loads. *Reviews of Geophysics*, 10(3):761–797.

Groh, A., Ewert, H., Scheinert, M., Fritsche, M., Rülke, A., Richter, A., Rosenau, R., and Dietrich, R. (2012). An investigation of glacial isostatic adjustment over the Amundsen Sea sector, West Antarctica. *Global and Planetary Change*, 98:45–53.

Khan, S. A., Sasgen, I., Bevis, M., van Dam, T., Bamber, J. L., Wahr, J., Willis, M., Kjær, K. H., Wouters, B., Helm, V., et al. (2016). Geodetic measurements reveal similarities between post–Last Glacial Maximum and present-day mass loss from the Greenland ice sheet. *Science advances*, 2(9):e1600931.

Leslie, A. G., Smith, M., Soper, N., Higgins, A., Gilotti, J., and Smith, M. (2008). Laurentian margin evolution and the caledonian orogeny—a template for scotland and east greenland. *The Caledonides of Greenland: Evolution of the Northeast Margin of Laurentia. Geological Society of America, Memoirs*, 202:307–343.

Melini, D., Gegout, P., Midi-Pyrenees, O., and Spada, G. (2015). a Regional ElAstic Rebound calculator.

Murton, J. B., Peterson, R., and Ozouf, J.-C. (2006). Bedrock fracture by ice segregation in cold regions. *Science*, 314(5802):1127–1129.

Noël, B., Van De Berg, W., Van Meijgaard, E., Kuipers Munneke, P., Van De Wal, R., and Van Den Broeke, M. (2015). Evaluation of the updated regional climate model RACMO2. 3: summer snowfall impact on the Greenland Ice Sheet. *The Cryosphere*, 9(5):1831–1844.

Patchett, P., Bylund, G., and Upton, B. (1978). Palaeomagnetism and the Grenville orogeny: new Rb-Sr ages from dolerites in Canada and Greenland. *Earth and Planetary Science Letters*, 40(3):349–364.

Peltier, W. (2004). Global glacial isostasy and the surface of the ice-age Earth: the ICE-5G (VM2) model and GRACE. *Annu. Rev. Earth Planet. Sci.*, 32:111–149.

Ran, J., Vizcaino, M., Ditmar, P., van den Broeke, M. R., Moon, T., Steger, C. R., Enderlin, E. M., Wouters, B., Noël, B., Reijmer, C. H., et al. (2018). Seasonal mass variations show timing and magnitude of meltwater storage in the Greenland Ice Sheet. *The Cryosphere*, 12(9):2981–2999.

Sneeuw, N. (1994). Global spherical harmonic analysis by least-squares and numerical quadrature methods in historical perspective. *Geophysical Journal International*, 118(3):707–716.

Srokosz, M. and Bryden, H. (2015). Observing the atlantic meridional overturning circulation yields a decade of inevitable surprises. *Science*, 348(6241):1255575.

Sun, Y., Riva, R., and Ditmar, P. (2016). Optimizing estimates of annual variations and trends in geocenter motion and J2 from a combination of GRACE data and geophysical models. *Journal of Geophysical Research: Solid Earth*, 121(11):8352–8370.

Wahr, J., Molenaar, M., and Bryan, F. (1998). Time variability of the Earth's gravity field: Hydrological and oceanic effects and their possible detection using GRACE. *Journal of Geophysical Research: Solid Earth*, 103(B12):30205–30229.

Zhang, B., Wang, Z., Li, F., An, J., Yang, Y., and Liu, J. (2017). Estimation of present-day glacial isostatic adjustment, ice mass change and elastic vertical crustal deformation over the Antarctic ice sheet. *Journal of Glaciology*, 63(240):703–715.